Supporting Information

Understanding the Cathode Electrolyte Interface Formation in Aqueous Electrolyte by Scanning Electrochemical Microscopy

Shuai Liu [a,b], Dongqing Liu *[a,c], Shuwei Wang [a,b], Xingke Cai [d], Kun Qian [a,b,e], Feiyu Kang [a,b,e], Baohua Li *[a]

[a] Shenzhen Key Laboratory on Power Battery Safety Research and Shenzhen Geim Graphene Center，Graduate School at Shenzhen, Tsinghua University, Shenzhen 518055, China.

[b] Laboratory of Advanced Materials, School of Materials Science and Engineering, Tsinghua University, Beijing 100084, P.R.China.

[c] Sunwoda Electronic Co., Ltd., Baoan District, Shenzhen 518055, P.R.China.

[d] Institute for Advanced Study, Shenzhen University, Shenzhen, Guangdong 518060, P. R. China.

[e] Shenzhen Environmental Science and New Energy Technology Engineering Laboratory, Tsinghua-Berkeley Shenzhen Institute, Shenzhen 518055, P. R. China.

* Corresponding author.

E-mail: libh@mail.sz.tsinghua.edu.cn (Baohua Li).

E-mail: liu.dongqing@sz.tsinghua.edu.cn (Dongqing Liu).

Experiment

Preparation of cathode electrode: the cathode electrode was prepared from a mixture of 80 wt% active material ($LiMn_2O_4$, MTI Corporation). 10 wt% conductive additive (super P) and 10 wt % binder polyvinylidene fluoride (PVDF). These materials in proportion were dissolved in n-methyl pyrrolidone (NMP) and stirred for 6 h at room temperature. And then the slurry was pasted onto the glassy carbon electrode and dried in oven at 60℃ for 6h.

Preparation of electrolyte: the mixed slat system "water-in-bisalt" consists of 21 m (mol salt in kg solvent, abbreviated as "m") lithium bis(trifluoromethanesulfonyl)imide (LiTFSI, DoDoChem, 99.8%) and 7 m lithium trifluoromethanesulfonate (LiTOf, Macklin, 98%). The salt in proportion was dissolved in water with 20 mmol/L $K_3Fe(CN)_6$ and 100 mmol/L KCl, in which $K_3Fe(CN)_6$ was used as redox mediator and KCl was added improve the electrolyte conductivity.

Material characterization: the morphology of electrode was studied by field emission scanning electron microscopy (FE-SEM, HITACH S4800) with an accelerating voltage of 5kV, and high resolution transmission electron microscope (HRTEM, TECNAIG2F30). The structure of $LiMn_2O_4$ was analyzed by X-ray Diffraction (XRD, Bruker D8 Advance). The surface composition was studied by X-ray photoelectron spectroscope (XPS, PHI 5000 Versa Probe II with Al Kα radiation).

Electrochemical characterization: the electrochemical measurements were carried out on Scanning Electrochemical Microscopy (SECM, Model 470, Bio-Logic SAS). Four electrodes set up was used, i.e. the Pt microelectrode with 15 μm diameter as one working electrode, the substrate with $LiMn_2O_4$ cathode material as the other working electrode, a Pt counter electrode and Ag/AgCl reference electrode. Cyclic voltammetry experiments with three electrode configuration were used to study the cycle performance of $LiMn_2O_4$ substrate from 0.4 to1.5 V vs. Ag/AgCl, and to determine the redox potentials of redox mediator $K_3Fe(CN)_6$ from 0.0 to 0.8 V vs. Ag/AgCl. The

sweep rate was 2 mV/s for the LMO electrode substrate and 1 mV/s for the Pt probe. Approach curve was used to study the conductivity of LMO substrate and determine the location of the probe for area scan. The approach curves were recorded at a step size of 2 μm in the z-axis direction. The area scan was performed with the probe approximately 20μm above the surface. The scanned area is 150 μm × 150 μm with 10 μm step in the x axis and y axis directions.

The SEM images and XRD pattern of the pristine LMO material reveal the micron size primary particles with cubic spinel crystal structure (space group $Fd\bar{3}m$) in **Figure S1**.

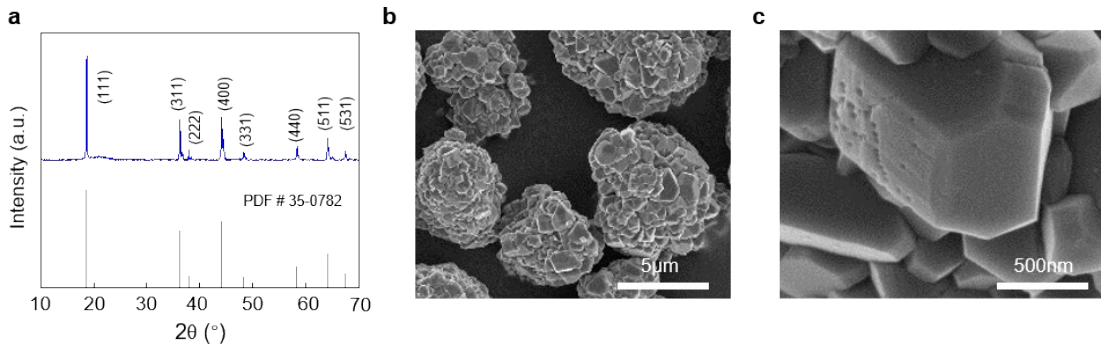

Figure S1. (a) XRD of pristine $LiMn_2O_4$. (b) and (c) SEM images of pristine $LiMn_2O_4$.

The LMO substrate was cycled between 3.5 V and 4.7 V at a sweep rate of 2 mV/s. The characteristic redox peaks of 4.52 V/4.34 V and 4.08 V/3.96 V were observed, shift positively due to the concentrated electrolyte [1, 2] (**Figure S2**a). The capacity faded obviously especially in the first ten cycles, mainly due to Mn dissolution from non-aqueous LIBs research experience [3, 4]. EIS were applied to study the impedance change of the LMO substrate at different cycles (**Figure S2**c). The ohmic resistance decrease, while the sum of interface and charge transfer resistance, and diffusion resistance increase with cycles, indicating the increase of polarization [5].

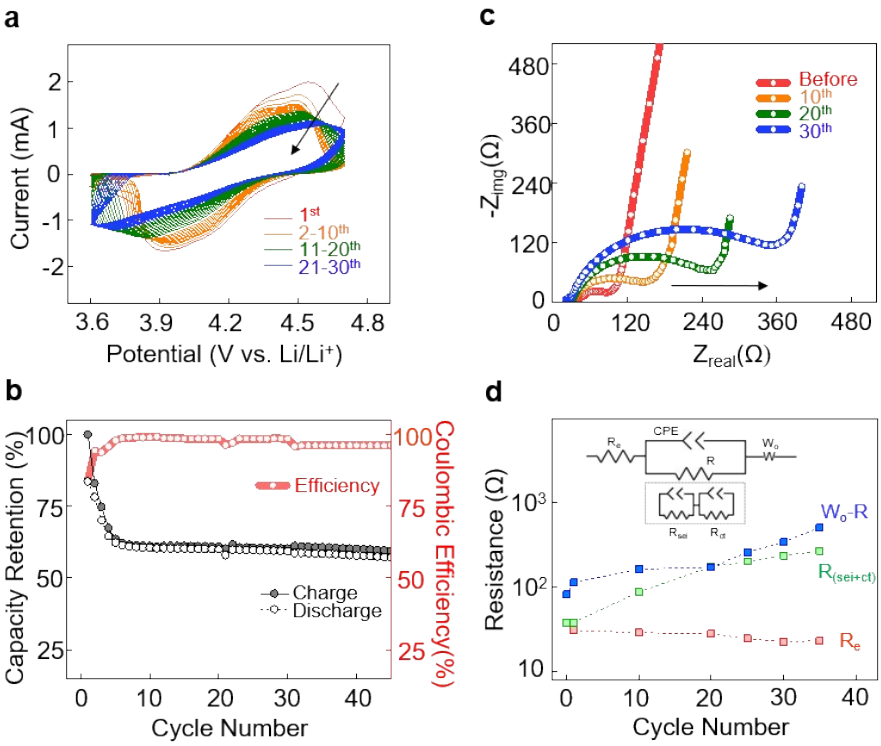

Figure S2. (a) Cyclic voltammograms of the LMO electrode from 1st to 30th cycles between 3.6 V and 4.7 V vs. Li/Li+. (b) the capacity retention and coulombic efficiencies with cycles. (c) Nyquist plots of LMO electrodes before cycling, after 10th, 20th, and 30th cycles. (d) the proposed equivalent circuit of EIS and change of fitting results with cycle number.

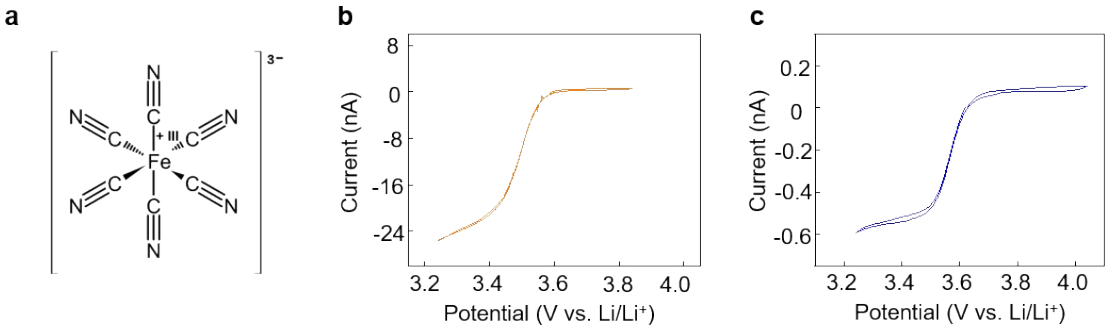

Figure S3. (a) Chemical structure of $[Fe(CN)_6]^{3-}$. Cyclic voltammograms of Pt electrode scanned at 1 mV s^{-1} in the (b) 20 mM $K_3[Fe(CN)_6]$ electrolyte and (c) 4 mM ($K_3[Fe(CN)_6]$)/21 m LiTFSI and 7 m LiOTf electrolyte.

Figure S4 show the SECM approach curve with the real measured feedback current. During the area scan, the probe was locked at about d = -50 μm position. The thickness

of CEI is ~ 10 nm from the TEM image. Assuming the CEI thickness rise to 50 nm, at position d=-50μm, the feedback current I=-342.93926pA; and at position d=-49.95μm the corresponding I=-342.860134pA. The feedback current would change about ~0.07 pA, indicating the thickness changes of CEI has little effect on the feedback current evolution. The approach curve is roughly fitted by equation $I = Intercept + B_1 \cdot d + B_2 \cdot d^2 + B_3 \cdot d^3 + B_4 \cdot d^4$.

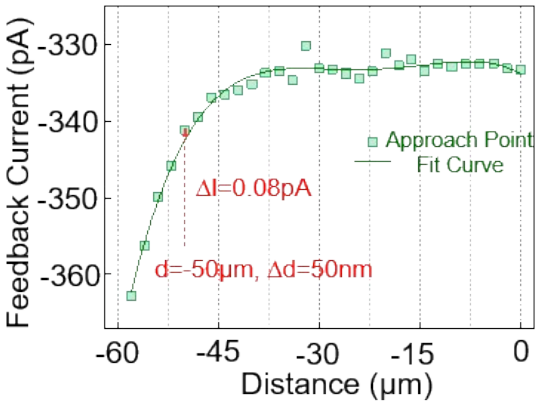

Figure S4. SECM approach curve towards the fresh $LiMn_2O_4$ electrode substrate.

Table S1. List of the parameter values for the feedback fit curve.

R-Square: 0.982	Value	Standard Error
Intercept	-333.84	0.77
B_1	-0.51	0.19
B_2	-0.051	0.014
B_3	-0.0018	3.58E-4
B_4	-2.06E-5	3.06E-6

The root mean square roughness S_q by definition is the root mean square average of the measured height deviations taken within the scan area. Here it's refers to the root mean square average of the measured feedback current deviations of the scanned area and it

can be expressed by the following equation:

$$S_q = \sqrt{\frac{1}{MN}\sum_{j=1}^{N}\sum_{i=1}^{M}\left[I(x_i, y_j) - I_{avg}\right]^2} \tag{S1}$$

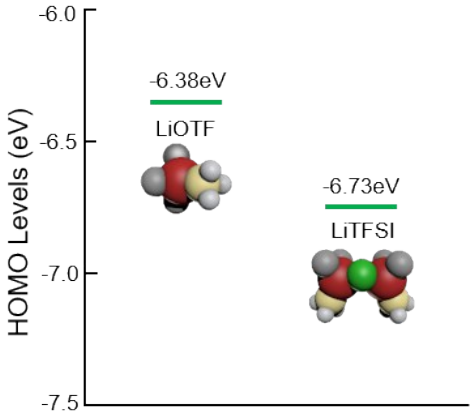

Figure S5. Highest occupied molecular orbital (HOMO) levels of LiTFSI and LiOTf.

Figure S6a shows the cycling performance of the $LiMn_2O_4$ electrode in the 28 m LiTOf electrolyte. Two characteristic redox peaks of 4.34V/4.12V and 4.47V/4.27V were observed. TEM was applied to characterize the morphology the cycled LMO electrode with the images taken from three separate places as shown in **Figure S6**b-d. An amorphous layer with the thickness of ~10nm was formed on the LMO surface after 60 cycles.

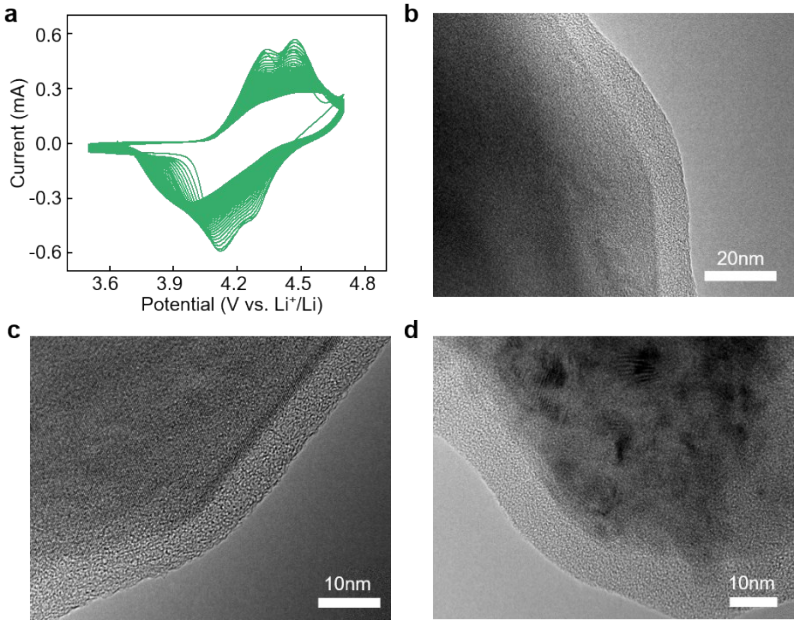

Figure S6. **a** Cyclic voltammograms of the LMO electrode in the 28 m LiTOf electrolyte from 1st to 60th cycles between 3.5 V and 4.7 V vs. Li/Li^+. **b-d** TEM images of the LMO electrode after cycling in the 28 m LiTOf electrolyte for 60 cycles.

XPS spectra of pure salt LiTOf and cycled LMO surface with CMC binder were carried out to clarify the peak assignment of F1s. In **Figure S7**b, a single peak CF_3 is observed for the LiTOf salt sample. The CF_3 peak of CEI overlaps with that of LiTOf, indicating that the CF_3 in the CEI originates from the salts of LiTFSI and LiTOf in the electrolyte. The CF_2 was ascribed to either damaged salt or PVDF binder according to literature. To clarify the doubt of PVDF binder signal in the $-(CF)_n-$ species, sodium carboxymethyl cellulose ($C_8H_{16}NaO_8$, CMC) with no F element was used as binder to prepare the LMO electrode. XPS depth profile was applied to study the chemical composition of the LMO interface after 60 cycles in the WIBs electrolyte as shown in **Figure S7**c. It can be seen that the three peaks of F1s remained even after prolonged sputtering, similar as the LMO sample with PVDF binder (**Figure 4**c). It indicates that the CF_2 signals are ascribed to the salt decomposition products rather than PVDF binder.

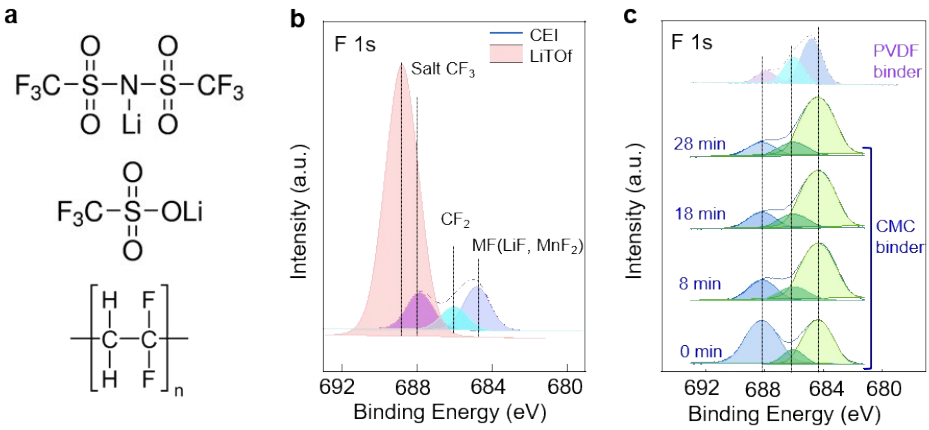

Figure S7. **a** Chemical structure of salt LiTFSI, LiTOf and binder PVDF. **b** XPS spectra of salt LiTOf and CEI of LMO in the WIBs electrolyte. **c** The peak assignment of F 1s and their change with sputtering time with CMC binder in comparation with PVDF binder.

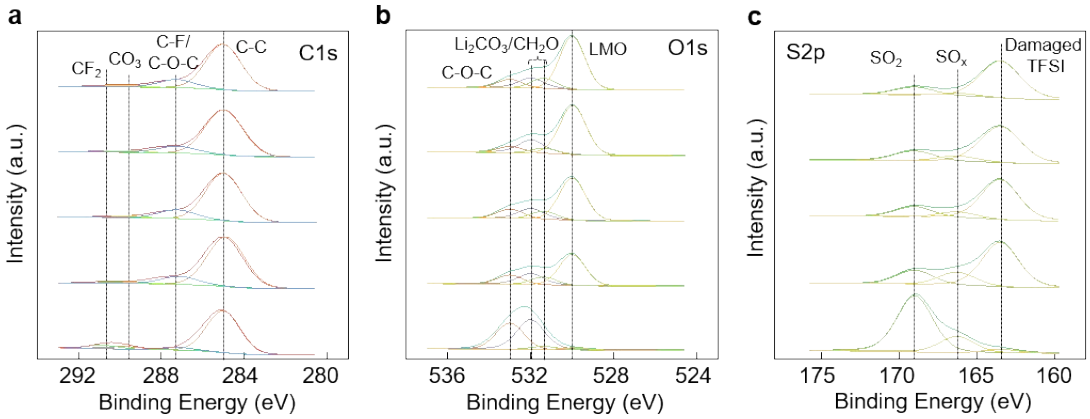

Figure S8. The peak assignment of (a) C 1s, (b) O 1s and (c) S 2p and their change with sputtering time.

References

1. F. Wang, Y. Lin, L. Suo, X. Fan, T. Gao, C. Yang, F. Han, Y. Qi, K. Xu and C. Wang, *Energy Environ. Sci.*, 2016, **9**, 3666-3673.

2. L. Suo, O. Borodin, W. Sun, X. Fan, C. Yang, F. Wang, T. Gao, Z. Ma, M. Schroeder, A. von Cresce, S. M. Russell, M. Armand, A. Angell, K. Xu and C. Wang, *Angew Chem. Int. Ed.*, 2016, **55**, 7136-7141.

3. M. Jeong, M.-J. Lee, J. Cho and S. Lee, *Adv. Energy Mater.*, 2015, **5**, 1500440.

4. M. Hirayama, H. Ido, K. Kim, W. Cho, K. Tamura, J. i. Mizuki and R. Kanno, *J. Am. Chem. Soc.*, 2010, **132**, 15268-15276.

5. A. Bhandari and J. Bhattacharya, *J. Electrochem. Soc*, 2017, **164**, A106-A127.